1   **Solar signal propagation: the role of gravity waves and stratospheric sudden warmings**

2   I. Cnossen[1], H. Lu[1], C.J. Bell[2], L.J. Gray[2] and M.M. Joshi[2]

3   [1]British Antarctic Survey, High Cross, Madingley Road, Cambridge CB3 0ET, United Kingdom

4   [2]University of Reading, Department of Meteorology, Reading RG6 6BB, United Kingdom

5   **Abstract**

6   We use a troposphere-stratosphere model of intermediate complexity to study the atmospheric

7   response to an idealized solar forcing in the subtropical upper stratosphere during Northern

8   Hemisphere (NH) early winter. We investigate two conditions that could influence the poleward and

9   downward propagation of the response: 1) the representation of gravity wave effects, and 2) the

10   presence/absence of Stratospheric Sudden Warmings (SSWs). We also investigate how the

11   perturbation influences the timing and frequency of SSWs. Differences in the poleward and

12   downward propagation of the response within the stratosphere are found depending on whether

13   Rayleigh friction (RF) or a gravity wave scheme (GWS) is used to represent gravity wave effects.

14   These are likely related to differences in planetary wave activity in the GWS and RF versions, as

15   planetary wave redistribution plays an important role in the downward and poleward propagation of

16   stratospheric signals. There is also remarkable sensitivity in the tropospheric response to the

17   representation of the gravity wave effects. It is most realistic for GWS. Further, tropospheric

18   responses are systematically different dependent on the absence/presence of SSWs. When only

19   years with SSWs are examined, the tropospheric signal appears to have descended from the

20   stratosphere, while the signal in the troposphere appears disconnected from the stratosphere when

21   years with SSWs are excluded. Different troposphere-stratosphere coupling mechanisms therefore

22   appear to be dominant for years with and without SSWs. The forcing does not affect the timing of

23 SSWs, but does result in a higher occurrence frequency throughout NH winter. Quasi-Biennial

24 Oscillation effects were not included.

25

26

1. Introduction

28 Variations in solar ultraviolet (UV) irradiance that take place over the 11-year solar cycle are known

29 to affect the upper stratosphere, where UV absorption by ozone takes place [Hood et al., 1993;

30 Haigh, 1994, 1996; Gray et al., 2010]. Increased UV irradiance at solar maximum produces not only

31 extra absorption directly, but also enhances the ozone concentration, making the equatorial upper

32 stratosphere 1.5-2.5 K warmer compared to solar minimum [Hood, 2004; Crooks and Gray, 2005;

33 Frame and Gray, 2010]. An even larger temperature signal associated with the 11-year solar cycle

34 has been observed in the high latitude regions of the lower stratosphere, which is particularly strong

35 during winter [Labitzke and Van Loon, 1988; Gray et al., 2004; Lu et al., 2009]. However, direct

36 effects of changes in solar irradiance appear to be too small to cause these high latitude signals

37 [Hood, 2004; Gray et al., 2009]. It has therefore been proposed that the solar UV forcing originating

38 in the upper equatorial stratosphere may propagate dynamically poleward and downward during

39 winter [Kodera and Kuroda, 2002; Matthes et al., 2004, 2006].

40 Kodera and Kuroda [2002] proposed a propagation mechanism involving the redistribution of

41 planetary wave forcing during Northern Hemisphere (NH) winter. They suggested that a region of

42 anomalously strong westerlies in the subtropical upper stratosphere/lower mesosphere during solar

43 maximum, in thermal wind balance with an enhanced pole-to-equator temperature gradient in the

44 upper stratosphere due to enhanced equatorial heating, may deflect planetary waves poleward. The

45 redistribution of planetary wave forcing towards higher latitudes further strengthens the polar

46 vortex in the subtropics, so that the zonal wind there becomes even more westerly. As the area of

47   anomalous westerly winds expands, this causes a further deflection of planetary waves, and so on,

48   so that the westerly anomaly gradually moves poleward and downward.

49   This mechanism was demonstrated in a simple idealized modelling study by Gray et al. [2004], who

50   imposed a small easterly anomaly in the subtropical upper stratosphere in early winter,

51   representative of solar minimum. This resulted in a consistently more disturbed winter with a

52   weaker vortex and earlier sudden warming events compared to their unforced integrations. Matthes

53   et al. [2004, 2006] successfully reproduced this same behaviour in the NH winter using a more

54   realistic full general circulation model, the Freie Universität Berlin Climate Middle Atmosphere

55   Model (FUB-CMAM), and obtained a pattern of poleward and downward propagation of zonal wind

56   anomalies, similar to observations. However, their modelled signal was much weaker than the

57   observed signals. Also other studies with full chemistry-climate models and realistic solar forcing

58   typically find signals that are weaker than seen in observations or at least at the lower end of

59   observed ranges of peak responses [e.g. Marsh et al., 2007; Austin et al., 2008]. Matthes et al. [2004]

60   argued that this could be due to the low variability produced by their model, as the amplitude of the

61   response to solar forcing may be related to the amplitude of inter-annual variability [see also Kodera

62   et al., 2003]. Kodera et al. [2003] further noted that the lower mesosphere subtropical jet was not

63   very well reproduced in these simulations, which they suggested may be due to the use of Rayleigh

64   friction as a crude parameterization of gravity wave forcings in the FUB-CMAM.

65   Rayleigh friction has long been the traditional approach to account for gravity wave effects, but is a

66   rather crude method. It simply assumes that a drag must be present that is proportional to the

67   ambient wind speed, with a height-dependent proportionality factor that is tuned such that a

68   realistic climatology is obtained. It has several drawbacks. Firstly, it is usually applied uniformly in

69   time, latitude and longitude, while real gravity wave sources and breaking events are likely to vary

70   with location and be intermittent [Fritts and Alexander, 2003]. Secondly, it assumes that wave

71   breaking always results in a drag on the mean wind, while in reality it may also accelerate winds in

72   some cases, depending on the wave characteristics and background wind itself. Thirdly, Rayleigh

73   friction does also not conserve momentum [Shepherd et al., 1996; Shepherd and Shaw, 2004].

74   A more sophisticated way to account for gravity wave effects that relieves some of these problems is

75   by means of a gravity wave parameterization that incorporates some representation of the wave

76   breaking process. This then determines where and when the waves break, and whether they

77   strengthen or weaken the winds as they do so, depending on the wave characteristics and

78   background winds. The first of such parameterizations were already formulated by Lindzen [1981]

79   and Dunkerton [1982], and since then have proven their value in many modelling studies [Fritts and

80   Alexander, 2003]. It has been shown recently that the use of a gravity wave parameterization, as

81   opposed to Rayleigh friction, can influence the modelled atmospheric response to a CO_2 forcing

82   [Sigmond et al., 2008; Cnossen et al., 2009; Sigmond and Scinocca, 2010].

83   There is some evidence that this may be the case for solar forcings as well. Shibata and Kodera

84   [2005] compared the results obtained with a traditional Rayleigh friction approach in their model to

85   those obtained with the parameterization described by Hines [1997]. They found that the Hines

86   parameterization produced a more realistic semi-annual oscillation (SAO). Differences in the

87   response to solar forcing between the Rayleigh friction and gravity wave scheme versions of their

88   model were therefore interpreted as being due to the absence/presence of the SAO. Further,

89   McCormack et al. [2007] showed that a reduction in Rayleigh friction strength resulted in a more

90   robust solar cycle modulation of the quasi-biennial oscillation (QBO), due to a larger solar cycle

91   variation in model dynamics near the stratopause. These studies thus indicate that the

92   representation of gravity wave effects can have consequences for the atmospheric response to solar

93   forcing.

94   The first objective of this study is to investigate such influences in more detail. We do this in an

95   extension of the study of Gray et al. [2004], using a similar zonal wind forcing in the subtropical

96   upper stratosphere. We use the Reading Intermediate General Circulation Model (IGCM3), which

4

97   includes the troposphere, so that we can follow the response further down in the atmosphere and

98   also assess tropospheric signals. In addition, our model integrations include a seasonal cycle, while

99   Gray et al. [2004] modelled perpetual January conditions. The focus of our analysis will be on the

100   poleward and downward propagation of the response in the Northern Hemisphere (NH), and we

101   investigate how this propagation is affected by the representation of gravity wave effects in the

102   model.

103   Our study also builds on the work of Haigh et al. [2005] and Simpson et al. [2009] who investigated

104   the tropospheric response to temperature forcings in the lower stratosphere. They used a simplified

105   version of the model we use, with a lower top (at ~18.5 hPa compared to 0.1 hPa in our model) and

106   no orography, and hence very weak planetary wave activity. They could therefore not study the

107   downward propagation of the response to (an idealized) solar forcing from the upper stratosphere,

108   where the solar UV and stratospheric ozone interaction takes place, to the lower stratosphere. We

109   take their work a step further, by prescribing a forcing in the upper subtropical stratosphere. This

110   allows us to study the downward and poleward propagation of the responses within the

111   stratosphere as well as the responses in the troposphere. We stress that we purely focus on

112   dynamical propagation mechanisms, as do Haigh et al. [2005], Simpson et al. [2009] and Gray et al.

113   [2004]. As a second, but related point of interest, we examine the role of Stratospheric Sudden

114   Warming (SSW) events in the response that is produced. SSWs occur in response to strong planetary

115   wave forcings, which can cause a temporary breakdown of the winter polar vortex, with zonal winds

116   reversing to easterlies and a corresponding warming as a result. As planetary waves are also thought

117   to be involved in solar signal propagation, linkages between the occurrence of SSW events and the

118   poleward and downward transport of solar signals may be expected. Indeed, the modelling study by

119   Gray et al. [2004] already showed that a subtropical forcing in the upper stratosphere affects both

120   the timing and frequency of SSWs. Here we re-examine their results with a different model,

121   including seasonality and the option to use a gravity wave scheme. We also look at the link between

122 SSWs and solar forcing from another angle, by studying the effects of the absence/presence of SSWs

123 on the responses obtained.

124 Both the sensitivities to gravity wave forcing and SSW occurrence that we find in the responses are

125 used as a tool to gain insights in the dynamical mechanisms that are responsible for the poleward

126 and downward propagation of the signal within the stratosphere, and for the communication of the

127 signal from the stratosphere into the troposphere. In addition, by quantifying the sensitivity of the

128 modelled responses to gravity wave effects and SSWs, we gain a better understanding of the

129 importance of modelling these aspects of the stratospheric climate correctly. This helps to

130 understand better why modelling studies so far have been unable to reproduce observed solar

131 signals with the correct strength and timing, and informs future modelling studies that attempt a

132 realistic simulation of solar cycle forcing.

133

134

135 **2. IGCM3 description and experimental setup**

136 2.1 IGCM3 description

137 The Reading Intermediate Global Circulation Model 3 (IGCM3) used in our experiments is a general

138 circulation model based on the spectral dynamical core of Hoskins and Simmons [1975]. It accounts

139 for a range of physical processes via parameterization schemes, as described in Forster et al. [2000].

140 These include a fast radiation scheme based on Morcrette [1990, 1991], a convection scheme based

141 on Betts [1986], a boundary layer scheme based on Louis [1986], and a slab ocean and land surface

142 scheme. In this sense, the IGCM3 is a general circulation model of intermediate complexity, bridging

143 the gap between simple dynamical models and full state-of-the-art GCMs.

144   The model has been used extensively in radiative forcing studies [Forster et al., 2000, Joshi and

145   Shine, 2003, Shine et al., 2003]. More recently, improvements to the model were made for the

146   investigation of stratospheric processes and their effect on climate, in particular by providing a

147   realistic simulation of the stratospheric mean state and variability [Bell et al., 2009]. The dynamical

148   core of the model is the same as that of the model used by Haigh et al. [2005] and Simpson et al.

149   [2009] for studying solar effects.

150   For this study, a T42 horizontal resolution (triangular truncation at wavenumber 42) was used with

151   38 vertical levels from 1000 to 0.1 hPa (16 levels in the troposphere, 19 levels in the stratosphere,

152   and 3 levels above 1 hPa). Also, a gravity wave scheme was implemented, used for some of the

153   simulations. The gravity wave scheme is based on Lindzen [1981] and Holton [1982], as described by

154   Barnes [1990] and Joshi et al. [1995], and conserves momentum. It includes both orographic and

155   non-orographic waves.

156   The orographic waves are assumed to be stationary (phase speed = 0 m/s) and have an amplitude

157   based on the sub-grid scale standard deviation of the topography, with a minimum value of 100 m,

158   and the zonal wind speed at the surface. The mean orography from the US Naval 1/6th degree

159   resolution dataset is used. A minimum value of 100 m was set to parameterize roughly residual

160   breaking in the uppermost layers of the model of waves from slowly moving features (including over

161   oceans). Two types of non-orographic waves, with phase speeds equal to the zonal wind speed at

162   ~500 hPa +20 m/s and -20 m/s, respectively, and a fixed amplitude (a tuneable parameter) are

163   included. This is a simplified representation of non-orographic gravity waves compared to the much

164   larger spectrum of waves that is often included in full climate models extending up to the

165   mesosphere (e.g. Garcia et al., 2007). These spectra sometimes have a latitudinal and seasonal

166   dependence as well, while our two waves are distributed homogeneously in space and time,

167   although some temporal and spatial dependence in phase speed is caused through variations in

168   zonal wind speed at 500 hPa. Our simplified approach is justified for the following reasons. Firstly,

169   our model does not extend into the mesosphere, so that there is little gain in including waves with

170   large phase speeds that would propagate through the stratosphere (and not break within the model

171   domain). Secondly, Barnes (1990) notes that the overall impact of a relatively broad spectrum of

172   waves on the zonal flow, even compared to just a single orographic mode, is not very large. And

173   finally, the "true" spectrum of gravity waves, and their seasonal and latitudinal variation, remains

174   not well known (e.g. Fritts and Alexander, 2003). Including more waves, with or without a

175   latitudinally and seasonally varying source, would thus not necessarily make our simulations more

176   realistic.

177

178   2.2 Experimental setup

179   Two control simulations were performed: one that used Rayleigh friction alone to account for gravity

180   wave forcing, and another one that used the gravity wave parameterization. These will be referred

181   to as RF-C and GWS-C, respectively. When only Rayleigh friction was used, this was employed over

182   the top six model levels (~0.1-3 hPa) with a time scale of 18 days at the lowest level, reducing to a

183   time scale of 3 days at the top level, over which winds were relaxed toward zero. The overall

184   strength of the Rayleigh friction was chosen such that the zonal mean temperature and zonal wind

185   climatologies for RF-C matched as closely as possible observed climatologies and the climatologies

186   obtained with GWS-C. This excludes as much as possible the effects of different background

187   climatologies on the response to the forcing. When the gravity wave scheme was used, a weak

188   Rayleigh friction was still retained at the top four model levels (~0.1-1 hPa) with a time scale of 19

189   days at the lowest level reducing to 4.7 days at the top level, to avoid spurious wave reflections from

190   the model top. The Rayleigh friction timescales for the RF and GWS simulations are shown in figure

191   1.

192   [[insert Figure 1 here]]

193   Two perturbed simulations were also performed and will be referred to as RF-P and GWS-P. The

194   perturbation consisted of a relaxation of the zonal winds in the subtropical upper stratosphere over

195   the top five model levels (~0.1-2 hPa), using a method similar to Rayleigh friction, but relaxing

196   towards -20 m/s. The forcing was applied at a central latitude of 12.5° over a width of 17.5°, with a

197   sinusoidal drop-off with latitude away from the central latitude, similar to that used by Gray et al.

198   [2004]. The forcing was only switched on for the duration of 1 month (30 days) in April for the

199   Southern Hemisphere (SH) and October for the Northern Hemisphere (NH), with a 10-day linear

200   ramp up and down in the months before and after to make them smooth in time. These temporary

201   forcings in early winter were chosen because forcing the model throughout the entire winter could

202   make it difficult to separate forcing from response, and because the stratosphere appears to be

203   particularly sensitive to solar perturbations originating from the subtropical upper stratosphere

204   during early winter [Gray et al., 2001; Matthes et al., 2004]. All simulations were run for 50 years

205   (18000 model days, with each month 30 days long for simplicity), in order to differentiate internal

206   model variability from the true dynamic response to the applied perturbations.

207   We did not force the model directly by changing the incoming irradiance and ozone concentration (a

208   seasonally varying ozone climatology based on Li and Shine [1995] was used in both control and

209   perturbed simulations). However, by forcing the zonal winds, a corresponding temperature

210   response in the forcing region is induced via thermal wind balance. The easterly forcing we apply

211   acts to reduce the meridional temperature gradient, resulting in a cooling cell over the equator and

212   a corresponding warming cell at higher latitudes. The structure of the forcing at 1-10 hPa is similar to

213   observed solar signals in October-November [e.g. Frame and Gray, 2010]. For simplicity and to aid a

214   straightforward explanation of the results, we assume the forced runs to represent solar minimum,

215   and the control runs to represent solar maximum. This approach has also been followed by other

216   studies investigating solar forcing effects, e.g. Gray et al. [2004]. The forcing we use results initially in

217   a larger zonal wind anomaly than is observed to be associated with the solar cycle: the model gives a

218   maximum zonal wind signal of 19 m/s during October, compared to 14 m/s in observations [Frame

219 and Gray, 2010]. However, this is justified, as our aim is not to reproduce solar signals exactly, but

220 rather to investigate the relevant propagation mechanisms, and the influences of gravity wave

221 effects and SSWs on the signal propagation.

222

223

224 **3. Results**

225 3.1 Control simulations

226 Figure 2 shows the October-November-December (OND) zonal mean temperature and zonal wind

227 climatologies, together with their standard deviation (shaded), for the GWS-C (left) and RF-C

228 (middle) simulations. The difference between the climatologies is also shown (right), with the

229 shading now indicating statistical significance. The climatologies for the two simulations are very

230 similar (which they were designed to be), and capture the main features of the observed zonal mean

231 temperature and wind structures. There are statistically significant differences between the

232 simulations, mainly in the stratosphere, but these differences are relatively small, and in particular

233 the zonal wind in the NH polar vortex matches to a high degree.

234   [[insert Figure 2 here]]

235 The GWS-C simulation gives slightly stronger inter-annual variability, with standard deviations in

236 temperature and zonal wind peaking at 3 K and 7 m/s, respectively, compared to 2.5 K and 5 m/s for

237 RF-C. The distributions of SSW events for the two simulations were determined based on the criteria

238 given in Charlton and Polvani [2007] and are shown in figure 3. They differ substantially, with the

239 peak of the SSW distribution occurring 1-2 months earlier for RF-C than for GWS-C. The SSW

240 distribution for GWS-C is in much better agreement with the observed distribution as reported by

241 Charlton and Polvani [2007], in particular for December and January. Note that the higher standard

242   deviations found for GWS-C are not directly related to a higher occurrence frequency of SSW events.

243   Rather, the higher standard deviations for GWS-C may be related to a higher total wave activity in

244   that simulation, as expressed by EP fluxes and EP flux divergence. The EP fluxes and EP flux

245   divergence for the GWS-C simulation are approximately 25% larger in the NH upper stratosphere in

246   OND than for RF-C.

247   [[insert Figure 3 here]]

248   Both model simulations are lacking a Quasi-Biennial Oscillation (QBO) and a realistic semi-annual

249   oscillation (SAO). The zonal wind at 30-50 hPa in the equatorial regions, where the QBO is normally

250   defined, is permanently easterly. The model does produce an SAO-like oscillation, but this is biased

251   towards easterlies, so that the oscillation is between very weak easterlies at the equinoxes (0 m/s

252   for RF; 0 to -6 m/s for GWS) and stronger easterlies during the solstices (-8 m/s for RF; -12 to -14 m/s

253   for GWS) rather than between easterlies and westerlies, as in observations.

254

255   3.2 Perturbed-control differences

256   Figure 4 shows sequences of differences between the perturbed and control integrations for GWS in

257   zonal mean temperature (left) and zonal wind (right) for 10-day intervals from the start of November

258   to the start of December. The temperature signal clearly moves poleward and downward from Nov

259   1-10 to Nov 21-30, until it nearly vanishes in Dec 1-10. The zonal wind signal propagates in

260   conjunction with the temperature signal, and there is also a response present in the troposphere

261   throughout November, consisting of a strengthening of zonal winds at 40°N and a weakening at

262   60°N. This roughly maps on to the Northern Annular Mode (NAM; Thompson and Wallace, 1998],

263   although we note that the modelled zonal wind response to our forcing is shifted ~5° northward

264   compared to the NAM dipole pattern observed in observational data, and that also the modelled

265   tropospheric jet is located up to 5° further north than the observed jet.

266   [[insert Figure 4 here]]

267   The poleward and downward movement of the temperature and zonal wind responses in the

268   stratosphere is dynamically consistent with the differences in EP flux and EP flux divergence, as

269   shown in the left-hand panels of figure 5. The right-hand panels of figure 5 show the transformed

270   Eulerian-mean [TEM; Andrews and McIntyre, 1976; Andrews et al., 1987] residual circulation, which

271   is a measure of the large scale meridional circulation that is induced by wave forcing, i.e. the Brewer-

272   Dobson (BD) circulation in the stratosphere.

273   [[insert Figure 5 here]]

274   In Nov 1-10 there is enhanced EP flux into the equator-ward flank of the polar vortex, and enhanced

275   EP flux convergence (near 40°N, 1 hPa). This signifies an increase of the wave forcing on the mean

276   flow, which acts to reduce the strength of the polar vortex. The enhanced wave forcing strengthens

277   the BD circulation in the area below, with a corresponding weakening in the region above the

278   enhanced wave forcing, effectively moving the circulation downwards. During Nov 11-20 and Nov

279   21-30, the upward EP flux into the polar vortex is further enhanced, while the centre of the activity

280   moves poleward. As a result the polar vortex is gradually being weakened from the outside equator-

281   ward flank to its inner core. The pair of positive and negative anomalies in the BD circulation also

282   moves poleward (from ~15°N in Nov 1-10 to ~60°N in Nov 21-30), although the negative anomaly is

283   no longer significant by Nov 21-30. In Dec 1-10 the system is recovering, but slightly overshooting, as

284   the EP flux is now reduced and EP flux divergence is enhanced compared to the control run. The

285   relatively weaker planetary wave forcing allows the polar vortex to strengthen again and weakens

286   the high latitude branch of the BD circulation. After Dec 1-10 (not shown), there is very little

287   significant signal remaining, indicating that the system has largely returned to its equilibrium state.

288   This is in agreement with the observations of Lu et al. [2009] that the NH signals in the polar

289   stratosphere have a life span of ~30-50 days, which is approximately the thermal relaxation

290   timescale in the lower stratosphere [Newman and Rosenfield, 1997].

291   The responses obtained from the RF simulations are of similar strength and show similar spatial

292   patterns in the stratosphere, but there are some differences in the timing of their poleward and

293   downward propagation. The RF response moves noticeably quicker towards the pole, reaching the

294   pole ~10 days earlier than the GWS response, with most of the downward propagation occurring

295   after that time.

296   In the troposphere, significant responses in the zonal wind are detected, which are substantially

297   different for RF and GWS, as shown in figure 6. There is relatively little movement of the

298   tropospheric signal over time, and it is most significant for November. Therefore only an average

299   response for November is shown. The zonal wind response for GWS consists of a weakening of the

300   zonal flow at 10-20°N at 100-200 hPa, a strengthening throughout the depth of the troposphere

301   centred at 40°N, and a weakening around 60°N at 250-500 hPa. This means that the core of the jet is

302   strengthened (see figure 2 for the jet position in the control simulations). The RF zonal wind signal

303   consists instead of a weakening from 15-20°N to 30-35°N through the depth of the troposphere and

304   a slight strengthening around 50°N. This represents a poleward movement of the tropospheric jet. In

305   both cases, the tropospheric responses do not appear to have directly descended from the

306   stratosphere. They remain roughly in place throughout November-December, regardless of the

307   temporal evolution of the stratospheric responses. At certain times they are therefore opposite in

308   sign to the stratospheric responses.

309   [[insert figure 6 here]]

310

311   3.3 Effects on timing and frequency distribution of SSWs

312   Because the GWS-C simulation produced an SSW distribution that is in better agreement with

313   observations than the RF-C simulation, the following sections will make use of the GWS results only.

314   Figure 7 compares the SSW distributions for the forced and control simulations. The overall shape of

13

315   the SSW distribution remains the same, but the forced run shows a consistent increase in SSWs

316   throughout winter compared to the control runs. This is in agreement with the finding by Gray et al.

317   [2004] that the rest of the NH winter becomes more disturbed as a result of an easterly forcing in

318   early winter in the subtropical upper stratosphere. However, a change in the timing of SSWs, as

319   found by Gray et al. [2004], can not clearly be seen in our results.

320   [[insert figure 7 here]]

321

322   3.4 SSW effects on the responses

323   To investigate the influence of SSWs on the tropospheric responses to the forcing, we separated the

324   data for the forced and control GWS simulations in years with and without SSWs during OND. For

325   both simulations, 12 years with SSWs and 38 years without SSWs were identified (this included three

326   years with an October SSW for GWS-C, which were not shown in figure 7). As noted previously, the

327   zonal wind response in the troposphere resembles a NAM-like pattern. Therefore a NAM-like index

328   was calculated to show the difference in the temporal evolution of the signal between the non-SSW

329   and SSW datasets. This index was calculated by subtracting the area-weighted average of the

330   geopotential height for 40-60°N from the area-weighted average for 60-90°N. These latitude bands

331   were chosen specifically to capture the responses most clearly. The geopotential height difference

332   was then normalized by subtracting the mean climatology for the control and perturbed datasets,

333   and dividing the result by the standard deviation of the combined datasets. Positive values

334   correspond to a positive NAM phase and negative values to a negative NAM, although our index is

335   not directly comparable to the NAM due to the different latitude bands used. Figure 8 shows

336   pressure-time sections of the response in the normalized geopotential height difference between

337   60-90°N and 40-60°N for the datasets with and without SSWs.

338   For years with SSWs, stronger poleward propagation of the response to the forcing takes place in the

339   stratosphere, so that the positive response in the stratospheric geopotential height difference

340   occurs earlier and is stronger as well. However, the overall propagation pattern of a positive signal

341   following a negative signal is similar for years with and without SSWs in the stratosphere. In

342   contrast, in the troposphere we find a negative signal around Nov 10 that appears to have

343   descended from the stratosphere for years with SSWs, while we find a signal of the opposite sign

344   around the same time, and in fact throughout the whole time interval presented, when years with

345   SSWs are excluded. The non-SSW tropospheric response does not appear directly connected to the

346   stratospheric response. When the entire dataset (SSW + non-SSW years) is processed, the signal

347   around Nov 10 is weaker, while the signal around Nov 20 is stronger. The signals from the two

348   conditions thus act to cancel each other out partly around Nov 10, while they add up around Nov 20.

349   [[insert figure 8 here]]

350

351

352   **4. Discussion**

353   4.1 Influences of gravity wave effects on solar signal propagation

354   Previous modelling studies have demonstrated that the representation of the stratosphere in a

355   general circulation model can influence the troposphere [e.g. Boville, 1984; Song and Robinson,

356   2004; Sigmond et al., 2008]. Here we build on those findings and show a specific influence of the

357   representation of gravity wave effects on the downward and poleward propagation of an idealized

358   solar forcing in the upper stratosphere. Differences between the GWS and RF simulations occur in

359   terms of the timing and extent of poleward and downward propagation of the responses in the

360   stratosphere, and also in general in the responses in the troposphere, even though the differences

361   between the RF and GWS simulations in terms of forcing and gravity wave representation are in the

362   (upper) stratosphere. The influences we find in the lower stratosphere and troposphere are thus

363   indirect.

364   The tropospheric zonal wind response for GWS is to some extent in agreement with observations by

365   Haigh et al. [2005], who found that the tropospheric jets are weaker and shift polewards for higher

366   solar activity. The GWS results did not show the change in jet position, but did show a change in

367   strength in the same sense, bearing in mind that our results are presented as solar minimum-

368   maximum conditions. The RF results on the other hand showed mostly a change in jet position, but it

369   moved poleward for solar minimum conditions compared to solar maximum, i.e. in the opposite

370   sense to the observations by Haigh et al. [2005]. For both RF and GWS the strength of the

371   tropospheric zonal wind signal is comparable to the strength of the observed anomalies reported by

372   Haigh et al., [2005]. The GWS pattern of a strengthening of the jet at 40°N with a weakening on

373   either side also matches the general pattern of the zonal wind signal observed by Frame and Gray

374   [2010], although their pattern is centred at 30-35°N, while the RF pattern does not. The GWS

375   simulations thus give a more realistic tropospheric response, in better agreement with observations.

376   Sigmond and Scinocca [2010] found that the sensitivity of the doubled CO_2 response to

377   parameterized orographic gravity wave drag [Sigmond et al., 2008] was largely due to differences in

378   the control climatologies. In our case, the differences in response to an idealized solar forcing do not

379   seem to be related to such differences, as the control climatologies were designed to be similar. We

380   can also exclude the possibility that the differences are related to different distributions of SSW

381   events (which were shown to differ more substantially), as excluding years with SSW events in OND

382   did not result in better agreement between the RF and GWS responses in OND (results not shown).

383   Shibata and Kodera [2005] interpreted the differences in response they found between their model

384   versions with Rayleigh friction and the Hines parameterization scheme in terms of the

385   absence/presence of an SAO. In our simulations however, we do not get a realistic SAO in either the

386 RF or GWS simulations. Therefore, while the SAO may have an influence in reality, it is not the

387 reason for the differences we find in our results. We will now explore two alternative explanations.

388 Firstly, it may be possible that the gravity wave forcing itself played a role in the propagation and

389 maintenance of the signal, by redistributing gravity wave momentum deposition, similar to how

390 planetary waves are thought to play a role in signal propagation by redistributing their momentum

391 deposition. We therefore examined the difference in gravity wave-induced accelerations between

392 the forced and control GWS runs, which revealed that these always acted to reduce the zonal wind

393 responses found (results not shown). So rather than amplifying the response, the direct effects of

394 changes in gravity wave momentum deposition acted to diminish the response, and we can

395 eliminate this possibility.

396 A second pathway for gravity wave effects to influence the response to our forcing is through

397 indirect effects on planetary waves. As noted, the EP fluxes and EP flux divergence were about 25%

398 larger in the NH upper stratosphere during OND for GWS-C compared to RF-C. This is consistent with

399 the finding by McLandress and McFarlane [1993] that longitudinal variations in gravity wave drag

400 (which would be missing in a Rayleigh friction approach) can enhance planetary wave amplitudes

401 and EP flux divergence. Considering the mechanism proposed by Kodera and Kuroda [2002], this

402 could explain why the stratospheric responses propagate differently for the GWS and RF versions of

403 the model, although the detail of the differences is not straightforward to explain.

404 The stronger planetary wave activity may also be responsible for the slightly stronger inter-annual

405 variability found for GWS. However, this small enhancement in inter-annual variability is not

406 sufficient to determine whether a lack of inter-annual variability is responsible for a too weak

407 response to solar forcing, as suggested by Matthes et al. [2004] and Kodera et al. [2003]. In terms of

408 strength, the responses obtained with the RF and GWS versions of the model are very similar.

409   In conclusion, our results indicate that it is important to model the planetary wave activity correctly,

410   and as gravity wave effects can modify this activity substantially, a more realistic representation of

411   gravity wave effects seems to be necessary to achieve this. The use of a gravity wave scheme does

412   not only affect stratospheric responses, but also the responses in the troposphere, which become

413   more realistic when the gravity wave scheme is used. We note that our model simulations, despite

414   making use of a gravity wave scheme, still do not necessarily provide a realistic description of gravity

415   wave effects, as strong assumptions were made on the characteristics of the waves. However, more

416   information on the global distribution of gravity wave effects is becoming available now [e.g.

417   Alexander et al., 2008] and future studies that attempt to realistically model the response to solar

418   forcing should take advantage of this.

419

420   4.2 Influences of SSW events on solar signals

421   Separating our data into years with and without SSW events in OND showed that responses are

422   substantially different under both conditions. Years with SSWs are highly disturbed, and typically

423   have a strong planetary wave forcing in the high latitude upper stratosphere, causing the polar

424   vortex to break down. Again, considering the Kodera and Kuroda [2002] mechanism of solar signal

425   propagation, we would expect poleward and downward propagation to be enhanced under such

426   conditions, and that is indeed what we observe. During years with SSWs a negative stratospheric

427   signal appears to descend down into the troposphere directly, becoming strongest there around Nov

428   10. This is followed by a positive stratospheric response, which also appears to descend down,

429   although the tropospheric response, while positive also, is not significant. In contrast, when years

430   with SSWs are excluded, the tropospheric signals are positive throughout and do not change in

431   conjunction with the time-varying changes in the stratosphere. The tropospheric signals appear

432   therefore more disconnected from the stratospheric signals in this case.

433   This does not mean that there is no connection between the phase of the NAM in the troposphere

434   and stratosphere when no SSWs are present, but suggests that different types of troposphere-

435   stratosphere coupling are dominant for disturbed (with SSWs) and quiet (no SSWs) conditions. The

436   mechanism responsible for the non-SSW signals is unlikely to be a direct tropospheric extension of

437   the mechanism responsible for the poleward and downward propagation of the stratospheric

438   signals. In other words, those tropospheric signals do not appear to be due to a change in planetary

439   wave forcing, and an associated change in a mean meridional circulation, extending from the

440   stratosphere into the troposphere, as this should have resulted in signals of the same sign in both

441   the stratosphere and troposphere. We therefore discuss two alternative coupling mechanisms.

442   The first mechanism involves changes in the tropospheric mean meridional circulation, forced by

443   changes in eddy momentum fluxes associated with synoptic waves within the troposphere [Simpson

444   et al., 2009]. The changes in eddy momentum fluxes are brought about by changes in temperature

445   gradients and zonal wind accelerations at the tropopause, in response to changes in the lower

446   stratospheric temperature structure and flow. Simpson et al. [2009] demonstrated the above

447   mechanism by modelling the effect of an altered latitudinal temperature structure in the lower

448   stratosphere on the troposphere. They showed that the response slowly develops in the upper

449   troposphere, over about 10 days, and gradually spreads to the lower troposphere, with the main

450   response structure established after about 20 days.

451   In our results we do not see a clear downward movement of the signal from the upper troposphere

452   into the lower troposphere over time, even though our model is a more advanced version of the

453   model used by Simpson et al. [2009]. Also, in our experiments the stratospheric signal does not

454   penetrate down into the lower stratosphere when years with SSWs are excluded, while there is still

455   a clear tropospheric response. It is therefore unlikely that the above mechanism is responsible for

456   our tropospheric response, although it is still possible that tropospheric eddies are involved in

457   amplifying/maintaining the tropospheric response (see also Kushner and Polvani, 2004; Song and

458   Robinson, 2004], once initiated by some other process.

459   The second mechanism involves changes in the reflection of planetary waves by the stratosphere

460   back into the troposphere, where they are subsequently absorbed [Perlwitz and Harnik, 2003, 2004;

461   Shaw et al., 2010]. Perlwitz and Harnik [2004] argued that this mechanism becomes more important

462   when the polar vortex is strong, in particular the lower part of the vortex (~30 hPa), as more wave

463   activity in that case is reflected back into the troposphere, rather than being absorbed by the

464   stratosphere. They also found that it is important mainly on short timescales (up to 12 days).

465   This mechanism could potentially explain why we find a different tropospheric signal for years with

466   and without SSWs. During years with SSWs, troposphere-stratosphere coupling via reflection of

467   planetary waves would be weak, while the mechanism would be more important, resulting in

468   stronger coupling, during years without SSWs, when the polar vortex is stronger. This is consistent

469   with our finding that tropospheric signals of opposite sign appear or become enhanced for years

470   without SSWs, while no significant signal, or a signal with the same sign as that in the stratosphere

471   appears for years with SSWs.

472   Previous studies have shown that there is a strong coupling between the troposphere and

473   stratosphere associated with SSWs [Baldwin and Dunkerton, 2001; Charlton and Polvani, 2007], but

474   this appears to be a more direct coupling, with signals from the stratosphere apparently descending

475   down into the troposphere. This is indeed what we observe in our results with SSWs, although most

476   of the responses are not significant. This could be due to the fact that the datasets with SSWs are

477   much shorter than the datasets without SSWs, and within the SSW datasets the SSWs also occurred

478   at different times. This gives a noisier dataset and makes it harder to establish a significant response.

479   A second possibility is that our forcing during years with SSWs could be relatively less important to

480   the troposphere than it is during years without SSWs, due to the dominance of the SSW influence on

481   the troposphere-stratosphere coupling in years with SSWs.

482   Finally, we note that the tropospheric responses of the SSW and non-SSW are sometimes of the

483   opposite sign and can therefore act to cancel each other out. This could be a possible reason for

484   difficulties in establishing a significant tropospheric signal in observational data, as both disturbed

485   and undisturbed years are normally included.

486

487   4.3 QBO influences

488   The interaction between the QBO and solar forcing is still unclear. Some studies have found that

489   solar forcing influences the QBO [McCormack et al., 2007] or that the QBO affects solar signals

490   [Labitzke and Van Loon, 1988; Gray et al., 2004; Labitzke et al., 2006], while others find little

491   interaction [Austin et al., 2008]. Lu et al. [2009] and Ito et al. [2009] found that the effects of the

492   QBO on solar signal propagation occur predominantly in late winter.

493   Our results were obtained with permanently weak easterlies in the equatorial stratosphere, so that

494   any interactions between solar forcing and the QBO have not been considered. However, as we

495   focus on early winter, the absence of a QBO may not have had a large effect. Still, the QBO affects

496   the distribution of planetary wave activity, which plays a key role in the poleward and downward

497   propagation of the signal in the stratosphere. Inclusion of a realistic QBO could therefore in principle

498   modify our results somewhat. On a background of westerly winds in the equatorial stratosphere, an

499   easterly forcing should still have the effect of deflecting waves poleward, but the strength of the

500   signal and the timing and extent of poleward propagation might be different.

501

502

503   **5. Summary and conclusions**

504 Our results broadly confirm the mechanism for solar signal propagation in the stratosphere

505 proposed by Kodera and Kuroda [2002]. We find that, in agreement with their theory, the

506 redistribution of planetary wave activity can strengthen an initial forced signal, and transport it

507 polewards and downwards from the equatorial upper stratosphere. We find that the type of

508 representation of gravity wave effects in our model influences this process, changing the timing and

509 extent of poleward and downward signal propagation in the stratosphere. This takes place most

510 likely through indirect effects of gravity wave-induced accelerations on planetary waves. The results

511 obtained with the gravity wave scheme are more realistic than those obtained with Rayleigh friction,

512 as they are in better agreement with observed solar signals, in particular in the troposphere.

513 The GWS results also produce a more realistic distribution of SSW events. The absence/presence of

514 SSW events has an effect on the propagation of the response to our forcing, mainly in the

515 troposphere. For years with SSWs tropospheric signals appear to descend directly from the

516 stratosphere, while they appear more disconnected when SSW years are excluded. We suggest that

517 this is due to different types of troposphere-stratosphere coupling being active under conditions

518 with and without SSWs. Under quiet conditions, a signal in the troposphere of the opposite sign to

519 that in the stratosphere may be generated through small modifications in the reflection of planetary

520 waves back into the troposphere. Once initiated, this signal may be maintained and/or strengthened

521 locally through changes in eddy momentum fluxes. In contrast, under disturbed conditions, when

522 SSWs occur, the troposphere-stratosphere coupling occurs more directly, and the tropospheric

523 response is an extension of that in the stratosphere.

524 The forcing also increases the number of SSWs, but does not influence their timing, as found by Gray

525 et al. [2004]. We therefore confirm only part of the findings of Gray et al. [2004]. Their result that

526 earlier SSWs occurred when an easterly forcing in the subtropical upper stratosphere was applied

527 may have been related to the absence of a seasonal cycle in their model integrations.

528

532

533

534 **References**

535 Alexander, M.J., J. Gille, C. Cavanaugh, M. Coffey, C. Craig, T. Eden, G. Francis, C. Halvorson, J.

536 Hannigan, R. Khosravi, D. Kinnison, H. Lee, S. Massie, B. Nardi, J. Barnett, C. Hepplewhite, A. Lambert

537 and V. Dean (2008). Global estimates of gravity wave momentum flux from High Resolution

538 Dynamics Limb Sounder observations, *J. Geophys. Res., 113*(D15), D15S18.

539 Andrews, D.G., J.R. Holton and C.B. Leovy, 1987. *Middle atmosphere dynamics,* pp. 489, Academic

540 Press, London, UK.

541 Andrews, D.G. and M.E. McIntyre (1976). Planetary waves on horizontal and vertical shear: the

542 generalized Eliassen-Palm Relation and the mean zonal acceleration, *J. Atmos. Sci., 33*(11), 2031-

543 2048.

544 Austin, J., K. Tourpali, E. Rozanov, H. Akiyoshi, S. Bekki, G. Bodeker, C. Brühl, N. Butchart, M.

545 Chipperfield, M. Deushi, V.I. Fomichev, M.A. Giorgetta, L. Gray, K. Kodera, F. Lott, E. Manzini, D.

546 Marsh, K. Matthes, T. Nagashima, K. Shibata, R.S. Stolarski, H. Struthers and W. Tian (2008). Coupled

547 chemistry climate model simulations of the solar cycle in ozone and temperature, *J. Geophys. Res.,*

548 *113*(D11), D11306, doi: 10.1029/2007JD009391.

549 Baldwin, M.P. and T.J. Dunkerton (2001). Stratospheric harbingers of anomalous weather regimes,

550 *Science, 294*(5542), 581-584.

551   Barnes, J.R. (1990). Possible effects of breaking gravity waves on the circulation of the middle

552   atmosphere of Mars, *J. Geophys. Res., 95*(B2), 1401-1421.

553   Bell, C.J., L.J. Gray, A.J. Charlton-Perez and M.M. Joshi (2009). Stratospheric cimmunication of El Niño

554   teleconnections to European winter, *J. Clim., 22*(15), 4083-4096. doi:10.1175/2009JCLI2717.1.

555   Betts, A.K. (1986). A new convective adjustment scheme 1. Observational and theoretical basis, *Q. J.*

556   *R. Meteorol. Soc., 112*(473), 677-691.

557   Boville, B.A. (1984), The influence of the polar night jet on the tropospheric circulation in a GCM, *J.*

558   *Atmos. Sci., 41*(7), 1132-1142.

559   Charlton, A.J. and L.M. Polvani (2007). A new look at Stratospheric Sudden Warmings. Part 1:

560   Climatology and modelling benchmarks, *J. Clim., 20*(3), 449-469.

561   Cnossen, I., M.J. Harris, N.F. Arnold and E. Yigit (2009). Modelled effect of changes in the CO_2

562   concentration on the middle and upper atmosphere: Sensitivity to gravity wave parameterization, *J.*

563   *Atmos. Solar-Terr. Phys., 71*(13), 1484-1496. doi:10.1016/j.jastp.2008.09.014.

564   Crooks, S.A. and L.J. Gray (2005). Characterization of the 11-year solar signal using a multiple

565   regression analysis of the ERA-40 dataset, *J. Clim., 18*(7), 996-1015.

566   Dunkerton, T.J. (1982). Stochastic parameterization of gravity wave stresses, *J. Atmos. Sci., 39*(8),

567   1711-1725.

568   Forster, P.M., M. Blackburn, R. Glover and K.P. Shine (2000). An examination of climate sensitivity for

569   idealised climate change experiments in an intermediate general circulation model, *Clim. Dyn.,*

570   *16*(10-11), 833-849.

571   Frame, T.H.A. and L.J. Gray (in press, 2010). The 11-year solar cycle in ERA-40 data: an update to

572   2008, *J. Clim., xx*(xx), xx-xx.

573   Fritts, D.C. and M.J. Alexander (2003). Gravity wave dynamics and effects in the middle atmosphere,

574   *Rev. Geophys., 41*(1), 1003.

575   Gray, L.J., J. Beer, M. Geller, J.D. Haigh, M. Lockwood, K. Matthes, U. Cubasch, D. Fleitmann, G.

576   Harrison, L. Hood, J. Luterbacher, G. Meehl, D. Shindell, B. van Geel and W. White (2010, in press).

577   Solar influences on climate, *Rev. Geophys., xx*(xx), xx-xx.

578   Gray, L.J., S. Crooks, C. Pascoe, S. Sparrow and M. Palmer (2004). Solar and QBO influences on the

579   timing of stratospheric sudden warmings, *J. Atmos. Sci., 61*(23), 2777-2796.

580   Gray, L.J., S.J. Phipps, T.J. Dunkerton, M.P. Baldwin, E.F. Drysdale and M.R. Allen (2001). A data study

581   of the influence of the equatorial upper stratosphere on northern-hemisphere stratospheric sudden

582   warmings, *Q. J. R. Meteorol. Soc. 127*(576), 1985-2003.

583   Gray, L.J., S.T. Rumbold and K.P. Shine (2009). Stratospheric temperature and radiative forcing

584   response to 11-year solar cycle changes in irradiance and ozone, *J. Atmos. Sci., 66*(8), 2402-2417.

585   Gray, L.J., S. Sparrow, M. Juckes, A. O'Neill and D.G. Andrews (2003). Flow regimes in the winter

586   stratosphere of the northern hemisphere, *Q. J. R. Meteorol. Soc.129*(589), 925-945.

587   Haigh, J.D. (1996). The impact of solar variability on climate, *Science, 272*(5264), 981-984.

588   Haigh, J.D. (1994). The role of stratospheric ozone in modulating the solar radiative forcing of

589   climate, *Nature, 370*(6490), 544-546.

590   Haigh, J.D., M. Blackburn and R. Day (2005). The response of the tropospheric circulation to

591   perturbations in lower-stratospheric temperature, *J. Clim., 18*(17), 3672-3685.

592   Hines, C.O. (1997). Doppler-spread parameterization of gravity-wave momentum deposition in the

593   middle atmosphere. Part 1: Basic formulation, *J. Atmos. Solar-Terr. Phys., 59*(4), 371-386.

594   Holton, J.R. (1982). The role of gravity wave induced drag and diffusion in the momentum budget of

595   the mesosphere, *39*(4), 791-799.

596   Hood, L.L., 2004. Effects of solar UV variability on the stratosphere, in *Solar variability and its effects*

597   *on climate*, edited by Pap, J.M. and P. Fox, pp. 283-303, American Geophysical Union, Washington

598   DC, USA.

599   Joshi, M.M. and K.P. Shine (2003). A GCM study of volcanic eruptions as a cause of increased

600   stratospheric water vapor, *J. Clim., 16*(21), 3525-3534.

601   Joshi M.M., B.N. Lawrence and S.R. Lewis (1995). Gravity wave drag in 3D atmospheric models of

602   Mars*, J. Geophys. Res., 100*(E10), 21235-21245.

603   Hood, L.L., J.L. Jirikowic and J.P. McCormack (1993). Quasi-decadal variability of the stratosphere:

604   influence of long-term solar ultraviolet variations, *J. Atmos. Sci., 50*(24), 3941-3958.

605   Hoskins, B.J. and A.J. Simmons (1975). A multi-layer spectral model and the semi-implicit method, *Q.*

606   *J. R. Meteorol. Soc., 101*(429), 637-655.

607   Ito, K., Y. Naito, and S. Yoden (2009), Combined effects of QBO and 11-year solar cycle on the winter

608   hemisphere in a stratosphere-troposphere coupled system, *Geophys. Res. Lett.*, 36, L11804,

609   doi:10.1029/2008GL037117.

610   Kodera, K. and Y. Kuroda (2002). Dynamical response to the solar cycle, *J. Geophys. Res., 107*(D24),

611   4749.

612   Kodera, K., K. Matthes, K. Shibata, U. Langematz and Y. Kuroda (2003). Solar impact on the lower

613   mesospheric subtropical jet: a comparative study with general circulation model simulations,

614   *Geophys. Res. Lett., 30*(6), 1315. doi:10.1029/2002GL016124.

615   Kushner, P.J. and L.M. Polvani (2004). Stratosphere-troposphere coupling in a relatively simple

616   AGCM: The role of eddies, *J. Clim., 17*(3), 629-639.

617   Labitzke, K. and H. Loon van (1988). Associations between the 11-year solar cycle, the QBO and the

618   atmosphere 1. The troposphere and stratosphere on the Northern Hemisphere in winter, *J. Atmos.*

619   *Terr. Phys., 50*(3), 197-206.

620   Labitzke, K, M. Kunze, and S. Bronnimann (2006). Sunspots, the QBO and the stratosphere in the

621   North Polar Region - 20 years later, *Meteorol. Zeitschrift*, 15, 355-363.

622   Li, D. and K.P. Shine (1995). A 4-dimensional ozone climatology for UGAMP models, *UGAMP Internal*

623   *Report, 35*.

624   Lindzen, R.S. (1981). Turbulence and stress owing to gravity wave and tidal breakdown, *J. Geophys.*

625   *Res., 86*(NC10), 9707-9714.

626   Louis, J.F., 1986. *Forecast model research manual 3: physical parameterization,* European Centre for

627   Medium Range Weather Forecasts, Research Department, Reading UK.

628   Lu, H., L.J. Gray, M.P. Baldwin and M.J. Jarvis (2009). Life cycle of the QBO-modulated 11-year solar

629   cycle signals in the Northern Hemispheric winter, *Q. J. R. Meteorol. Soc., 135*(641), 1030-1043.

630   doi:10.1002/qj.419.

631   Marsh, D.R., R.R. Garcia, D.E. Kinnison, B.A. Boville, F. Sassi, S.C. Solomon and K. Matthes (2007).

632   Modeling the whole atmosphere response to solar cycle changes in radiative and geomagnetic

633   forcing, *J. Geophys. Res., 112*(D23), D23306, doi:10.1029/2006JD008306.

634   Matthes, K., Y. Kuroda, K. Kodera and U. Langematz (2006). Transfer of the solar signal from the

635   stratosphere to the troposphere: Northern winter, *J. Geophys. Res., 111*(D6), D06108.

636   doi:10.1029/2005JD006283.

637   Matthes, K., U. Langematz, L.J. Gray, K. Kodera and K. Labitzke (2004). Improved 11-year solar signal

638   in the Freie Universität Berlin Climate Middle Atmosphere Model (FUB-CMAM), *J. Geophys. Res.,*

639   *109*(D6), D06101. doi:10.1029/2003JD004012.

640   McCormack, J.P., D.E. Siskind and L.L. Hood (2007). Solar-QBO interaction and its impact on

641   stratospheric ozone in a zonally averaged photochemical transport model of the middle atmosphere,

642   *J. Geophys. Res., 112*(D16), D16109. doi:10.1029/2006JD008369.

643   McLandress, C. and N.A. McFarlane (1993). Interactions between orographic gravity wave drag and

644   forced stationary planetary waves in the winter Nortern Hemisphere middle atmosphere, *J. Atmos.*

645   *Sci., 50*(13), 1966-1990.

646   Morcrette, J.J. (1991). Radiation and cloud radiative properties in the European Centre for Medium

647   Range Weather Forecasts forecasting system, *J. Geophys. Res., 96*(D5), 9121-9132.

648   Morcrette, J.J. (1990). Impact of changes to the radiation transfer parameterizations plus cloud

649   optical properties in the ECMWF model, *Mon. Weather Rev., 118*(4), 847-873.

650   Newman, P.A. and J.E. Rosenfield (1997). Stratospheric thermal damping times, *Geophys. Res. Lett.,*

651   *24*(4), 433-436.

652   Perlwitz, J. and N. Harnik (2004). Downward coupling between the stratosphere and troposphere:

653   the relative role of wave and zonal mean processes, *J. Clim., 17*(24), 4902-4909.

654   Perlwitz, J. and N. Harnik (2003). Observational evidence of a stratospheric influence on the

655   troposphere by planetary wave reflection, *J. Clim., 16*(18), 3011-3026.

656   Shaw, T.A., J. Perlwitz and N. Harnik (submitted, 2010). Downward wave coupling between the

657   stratosphere and troposphere: the importance of meridional wave guiding and comparison with

658   zonal-mean coupling, *J. Clim., xx*(xx), xx-xx.

659   Shepherd, T.G., K. Semeniuk and J.N. Koshyk (1996). Sponge layer feedbacks in middle-atmosphere

660   models, *J. Geophys. Res., 101*(D18), 23447-23464.

661   Shepherd, T.G. and T.A. Shaw (2004). The angular momentum constraint on climate sensitivity and

662   downward influence in the middle atmosphere, *J. Atmos. Sci., 61*(23), 2899-2908.

663   Shibata, K. and K. Kodera (2005). Simulation of radiative and dynamical responses of the middle

664   atmosphere to the 11-year solar cycle, *J. Atmos. Solar-Terr. Phys., 67*(1-2), 125-143.

665   doi:10.1016/j.jastp.2004.07.022.

666   Shine, K.P., J. Cook, E.J. Highwood and M.M. Joshi (2003). An alternative to radiative forcing for

667   estimating the relative importance of climate change mechanisms, *Geophys. Res. Lett., 30*(20), 2047.

668   doi: 10.1029/2003GL018141.

669   Sigmond, M. and J.F. Scinocca (2010). The influence of the basic state on the Northern Hemisphere

670   circulation response to climate change, *J. Clim., 23*(6), 1434-1446. doi:10.1175/2009JCLI3167.1.

671   Sigmond, M., J.F. Scinocca and P.J. Kushner (2008). Impacts of the stratosphere on tropospheric

672   climate change, *Geophys. Res. Lett., 35*(12), L03704. doi:10.1029/2008GL033573.

673   Simpson, I.R., M. Blackburn and J.D. Haigh (2009). The role of eddies in driving the tropospheric

674   response to stratospheric heating perturbations, *J. Atmos. Sci., 66*(5), 1347-1365.

675   doi:10.1175/2008JAS2758.1.

676   Song, Y. and W.R. Robinson (2004). Dynamical mechanisms for stratospheric influences on the

677   troposphere, *J. Atmos. Sci., 61*(14), 1711-1725.

678   Thompson, D.W.J. and J.M. Wallace (1998). The Arctic Oscillation signature in the wintertime

679   geopotential height and temperature fields, *Geophys. Res. Lett., 25*(9), 1297-1300.

680

681   **Figure captions**

682   Figure 1. Rayleigh friction timescales used for the top levels of the RF and GWS simulations.

683   Figure 2. Zonal mean temperature (top) and zonal wind (bottom) climatologies for the GWS-C

684   simulation (left), the RF-C simulation (middle), and the difference between the GWS-C and RF-C

685   simulations (right) for OND. For the left and middle panels the shading indicates the standard

686   deviation. For the right panels the shading indicates statistical significance at the 95% (light shading)

687   and 99% (dark shading) level, as determined with a T-test.

688   Figure 3. Distribution of the occurrence frequency of SSW events for the RF-C and GWS-C

689   simulations and the observed SSW frequency from Charlton and Polvani (2007) based on the

690   average of the NCEP and ERA-40 occurrences.

691   Figure 4. Differences in the zonal mean temperature (left) and zonal wind (right) climatologies

692   between the GWS perturbed and control simulations for 10-day averages from Nov 1-10 to Dec 1-

693   10. Light shading indicates 95% statistical significance, and dark shading 99% statistical significance,

694   as determined with a T-test.

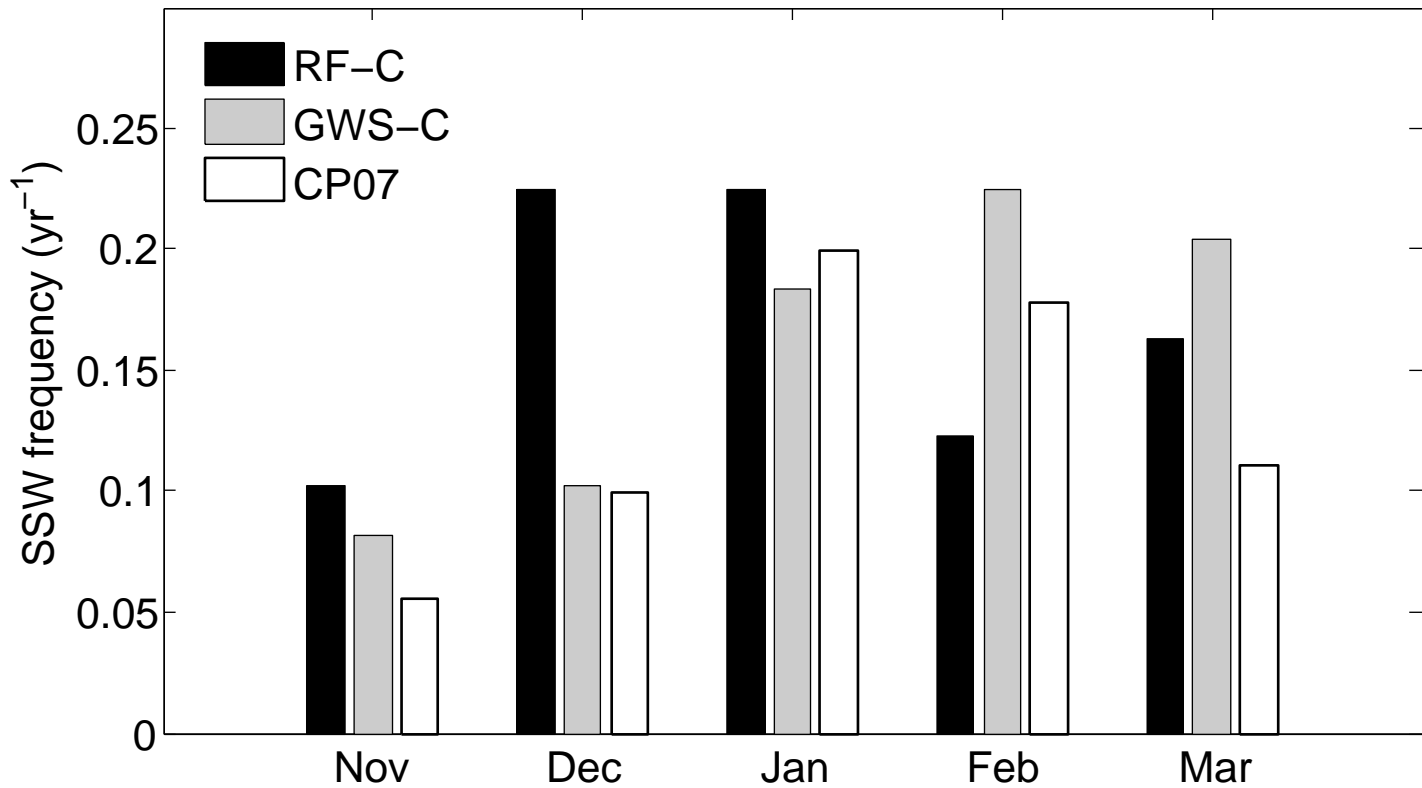695   Figure 5. Differences in the EP flux (arrows) and EP flux divergence (contours; left), scaled according

696   to the "acceleration" scaling defined by Gray et al. [2003], and TEM flow vectors (arrows) and

697   residual circulation (contours; right) climatologies between the GWS perturbed and control

698   simulations for 10-day averages from Nov 1-10 to Dec 1-10. EP flux vectors have units of m^2s^{-2}, with

699   a metric factor applied to give reasonable arrow lengths on the plot, and the EP flux divergence has

700   units of $ms^{-1}day^{-1}$. The TEM residual circulation has units of 10^9 kg/s and is scaled by $1/\sigma$, where $\sigma =$

701    $P/P_{surface}$, the TEM horizontal flow vector has units of ms^{-1}, and the TEM vertical flow vector has units

702   of mb $hour^{-1}$ and is also scaled by $1/\sigma$. A metric factor is applied to the flow vectors to give

703   reasonable arrow lengths on the plot. Light shading indicates 95% statistical significance, and dark

704   shading 99% statistical significance, as determined with a T-test.

705   Figure 6. Differences in the zonal mean zonal wind climatologies in the troposphere for the

706   perturbed and control simulations for GWS (left) and RF (right) for November. Light shading

707   indicates 95% statistical significance, and dark shading 99% statistical significance, as determined

708   with a T-test.

709   Figure 7. Distribution of the occurrence frequency of SSW events for the GWS for the control and

710   perturbed simulations.

711   Figure 8. Pressure-time section of the normalized geopotential difference between 60-90°N and 40-

712   60°N between the GWS perturbed and control datasets without SSWs (left) and with SSWs (right)

713   from Oct 10 to Dec 30. There are 12 years with SSWs and 38 years without SSWs in both GWS-C and

714   GWS-P. Light shading indicates 90% statistical significance, and dark shading 95% statistical

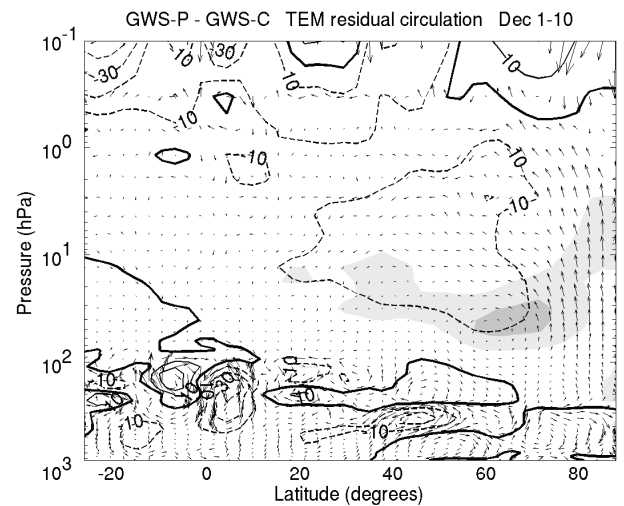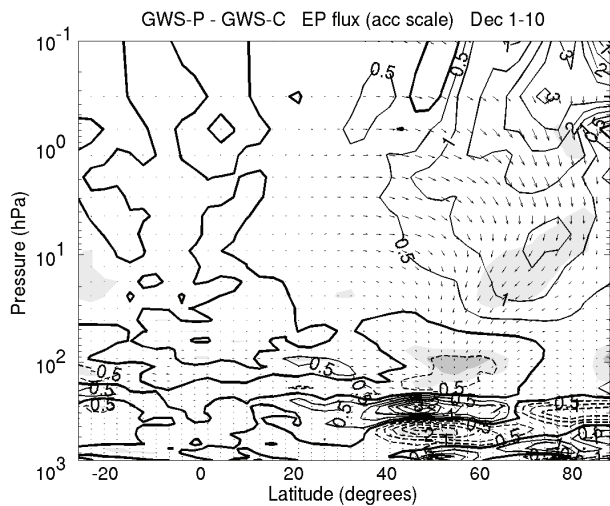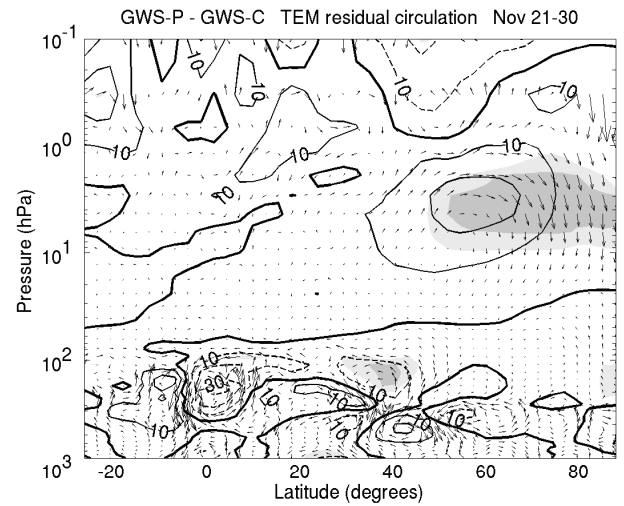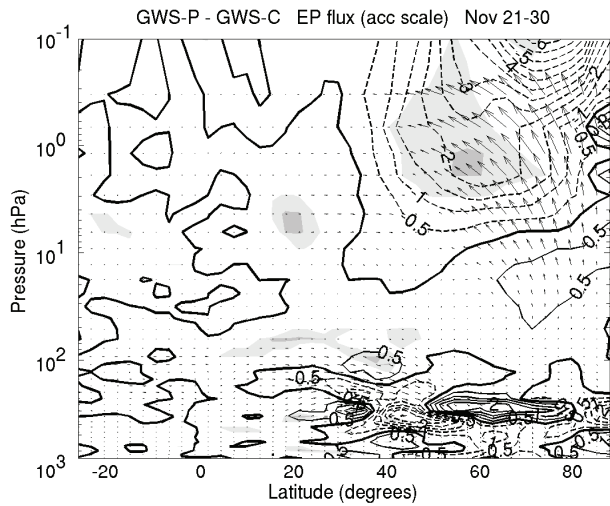715   significance, as determined with a T-test.

GWS-P - GWS-C   EP flux (acc scale)   Nov 1-10

GWS-P - GWS-C   TEM residual circulation   Nov 1-10

GWS-P - GWS-C   EP flux (acc scale)   Nov 11-20

GWS-P - GWS-C   TEM residual circulation   Nov 11-20

GWS-P - GWS-C   EP flux (acc scale)   Nov 21-30

GWS-P - GWS-C   TEM residual circulation   Nov 21-30

GWS-P - GWS-C   EP flux (acc scale)   Dec 1-10
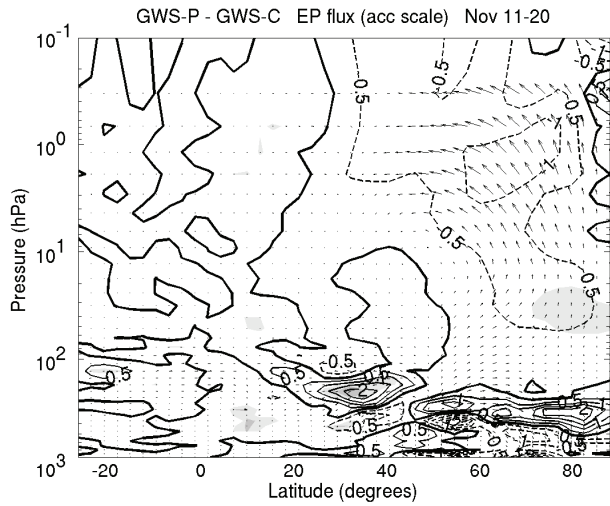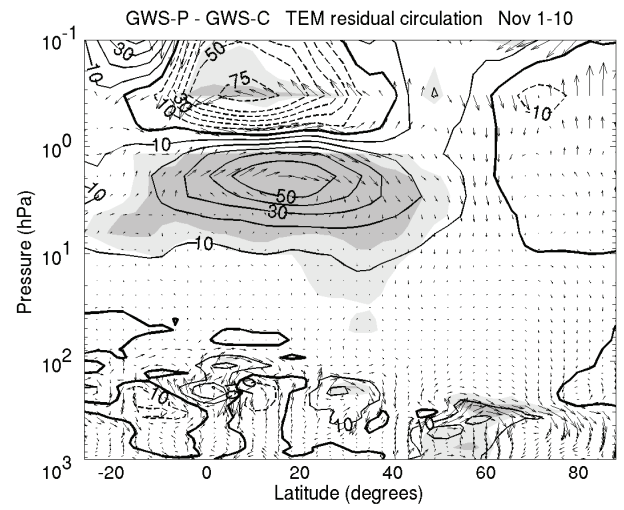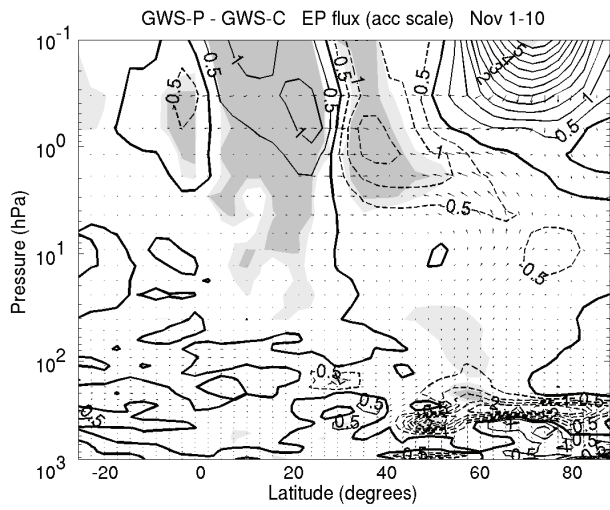
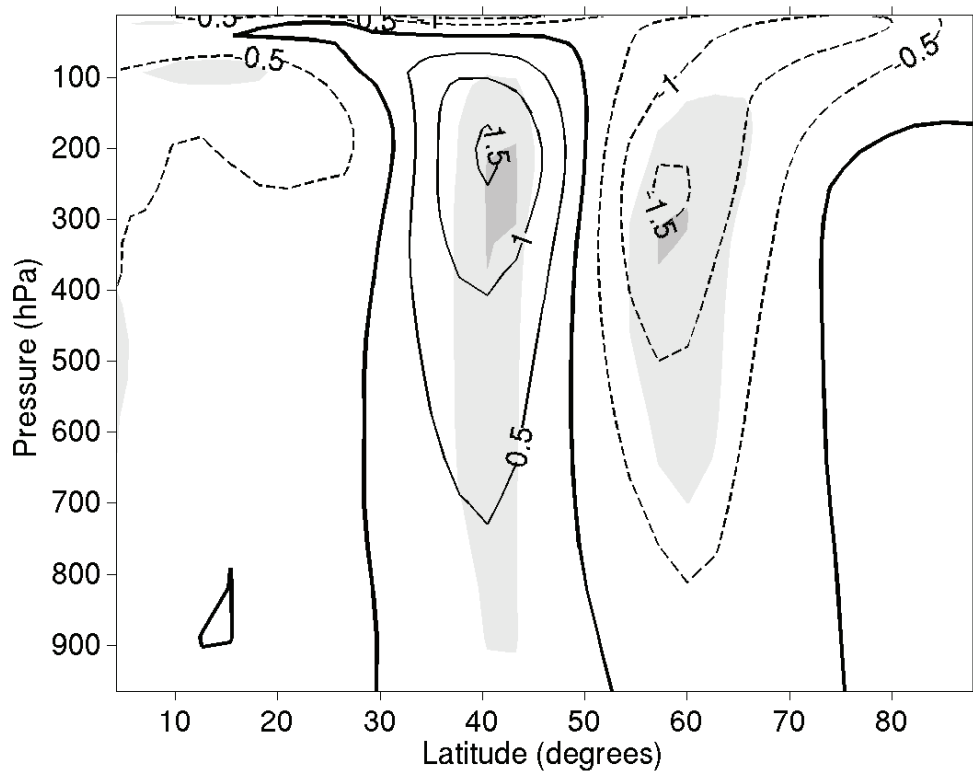GWS-P - GWS-C   TEM residual circulation   Dec 1-10
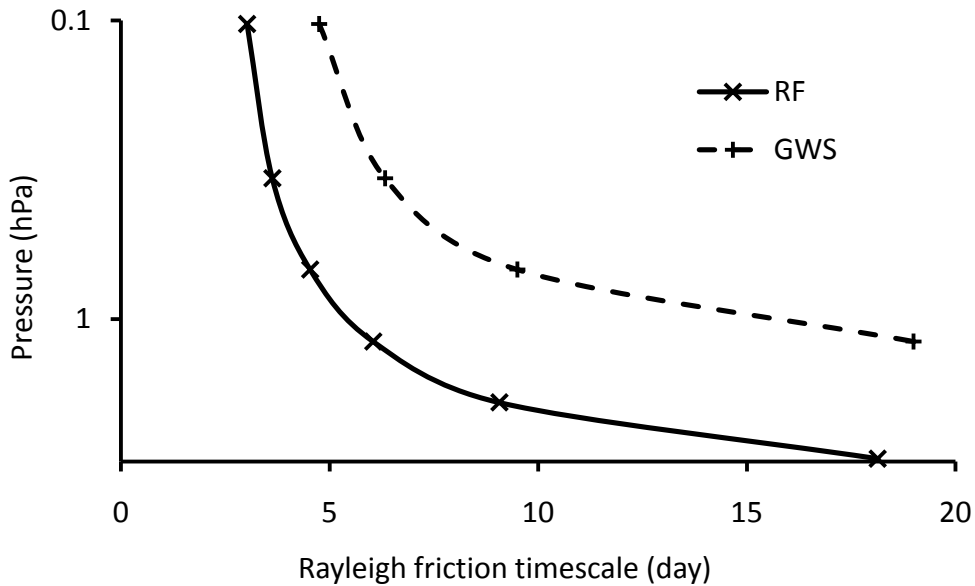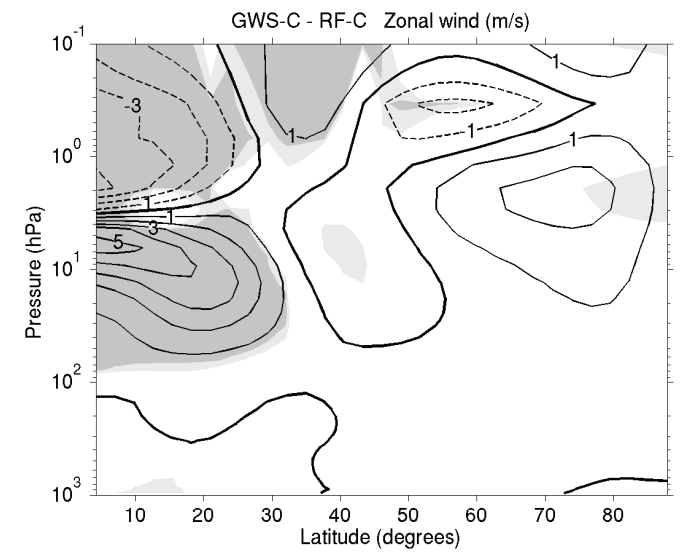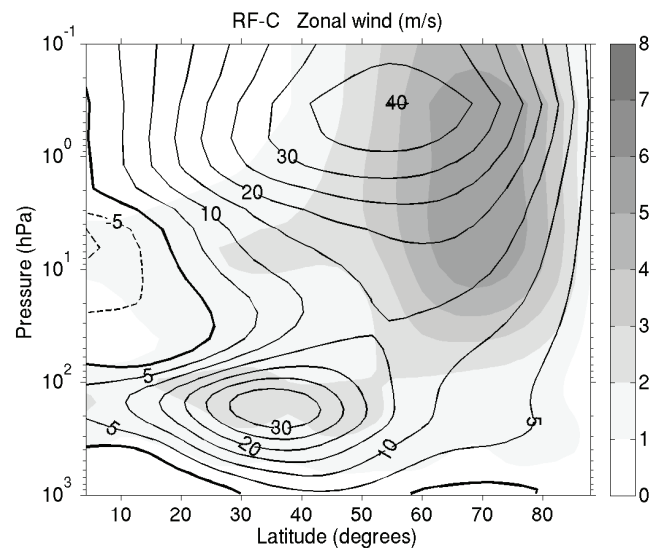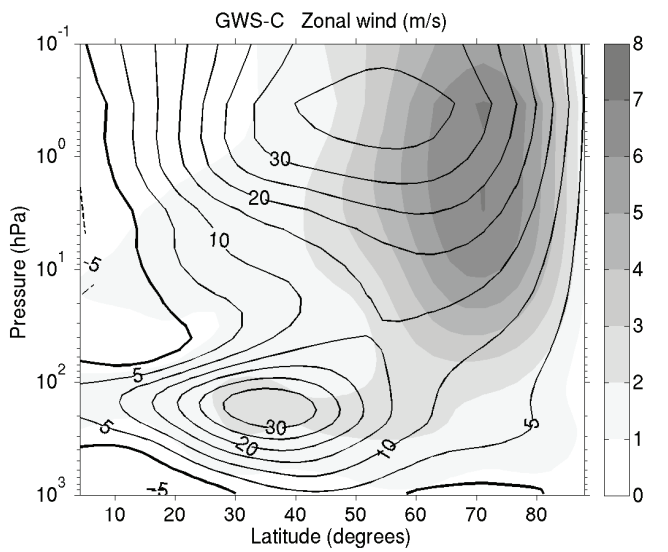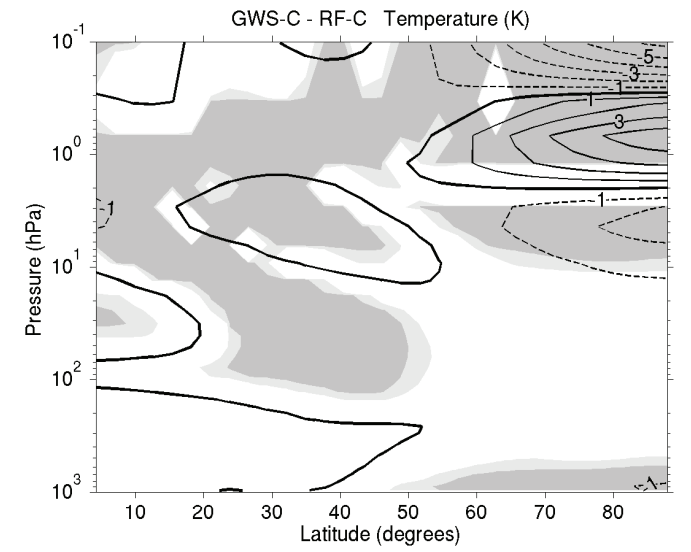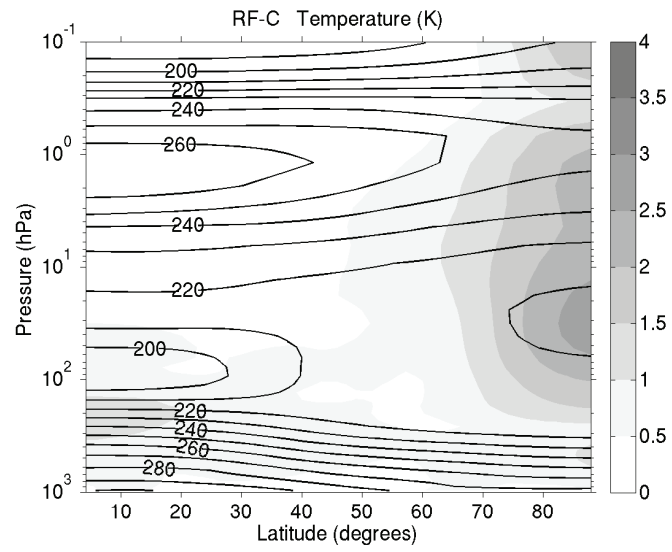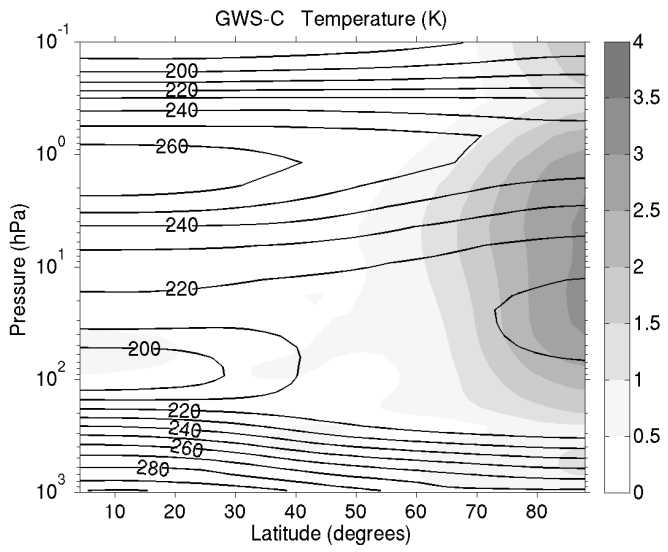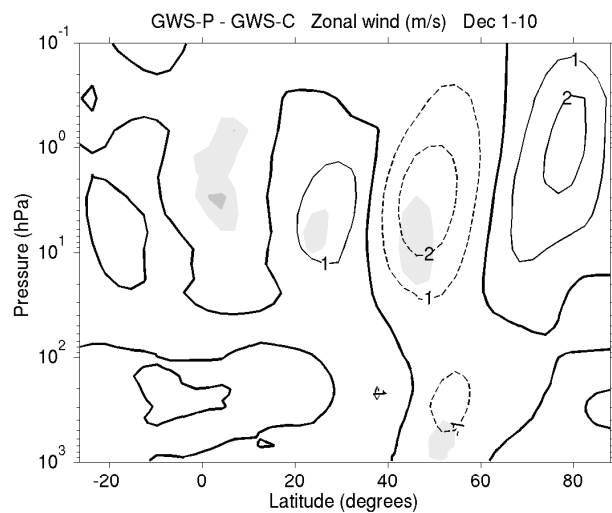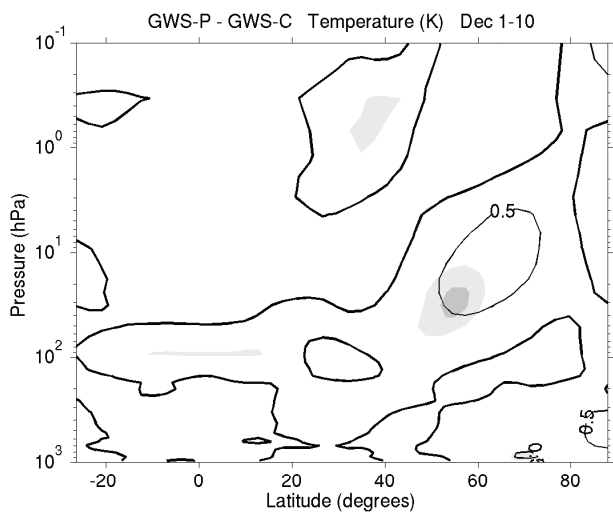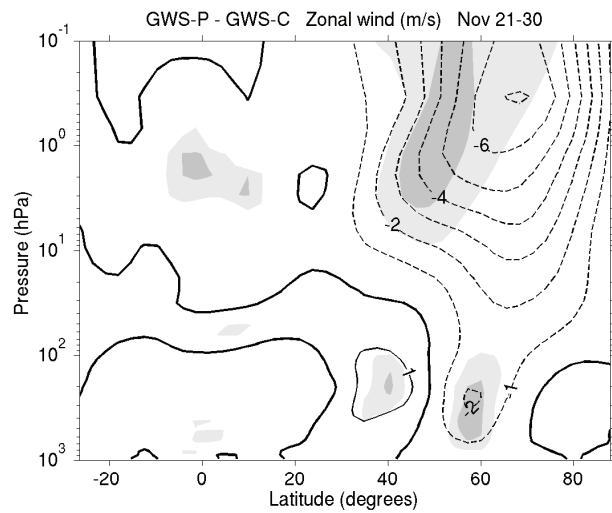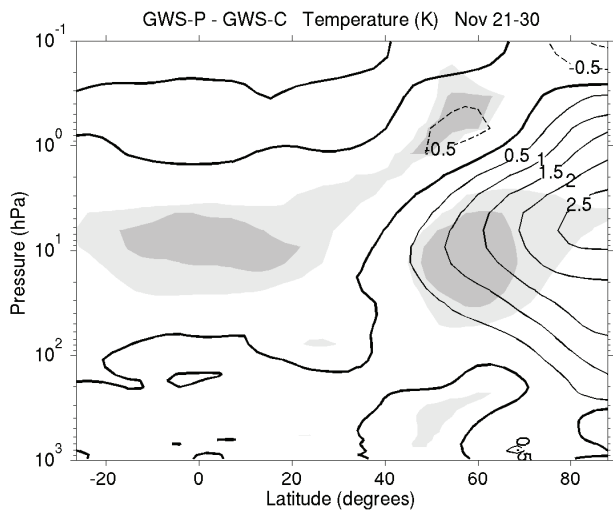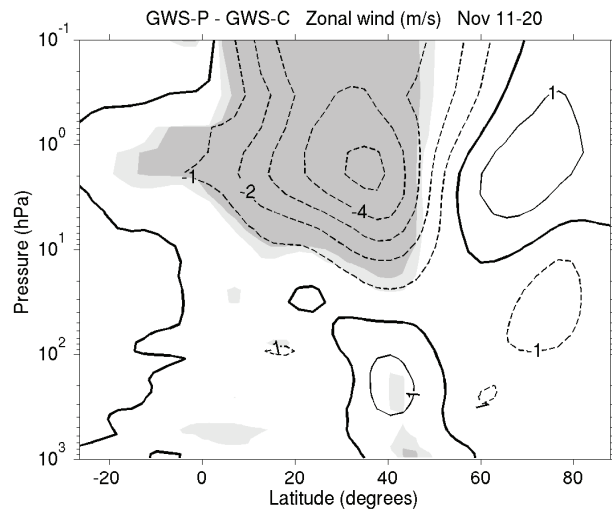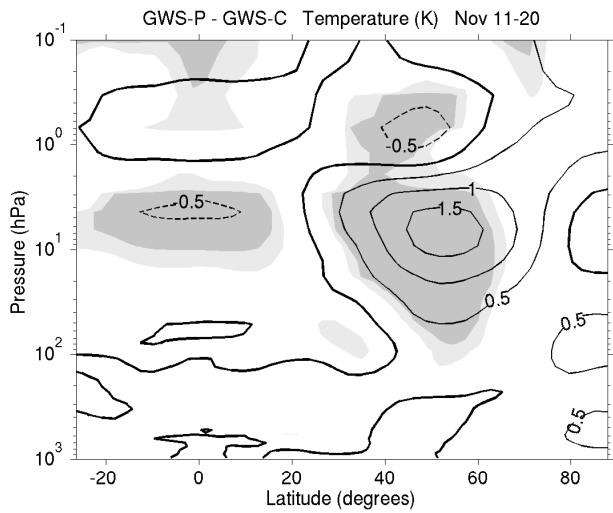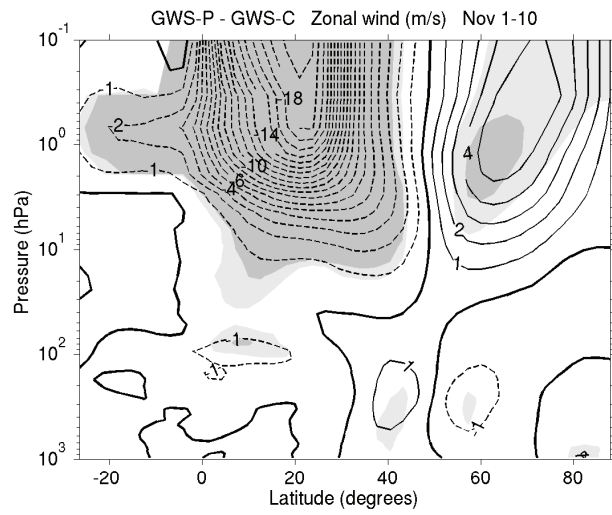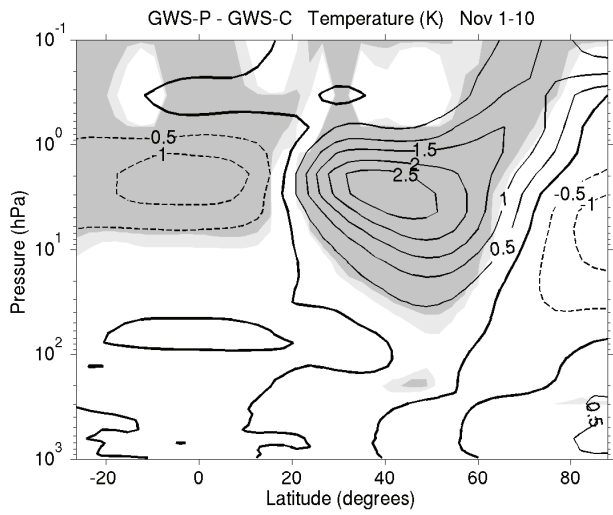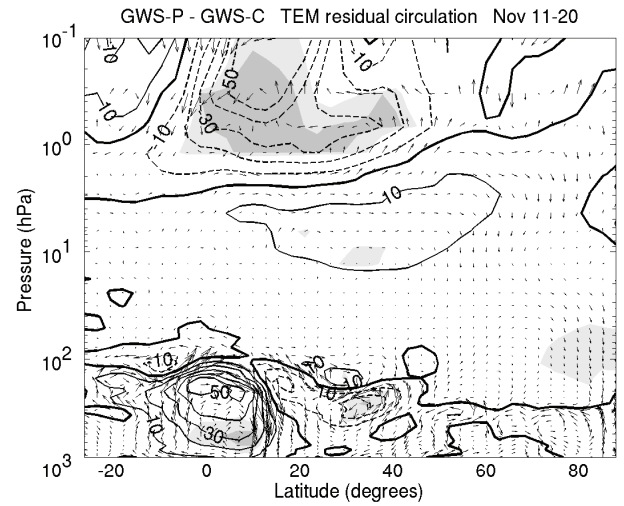
GWS-P - GWS-C   Zonal wind (m/s)   Nov

RF-P - RF-C   Zonal wind (m/s)   Nov

GWS-P - GWS-C   Geopotential height (normalized) at 60-90N - 40-60N   no SSW in Oct-Dec

GWS-P - GWS-C   Geopotential height (normalized) at 60-90N - 40-60N   SSW in Oct-Dec